Extracting and Predicting Multipath Profiles under High Mobility

Ghufran Baig¹, Changhan Ge¹, Lili Qiu¹,⁴, Yuanjie Li², Wangyang Li¹, Wei Sun¹, Jian He¹, Zhehui Zhang³, Songwu Lu³

¹ The University of Texas at Austin, Austin, TX, USA
 ² Tsinghua University, Beijing, P.R.China
 ³ University of California Los Angeles, Los Angeles, CA, USA
 ⁴ Microsoft Research Asia, Shanghai, P.R.China

ABSTRACT

The wireless signal propagates via multipath arising from different reflections and penetration between a transmitter and receiver. Extracting multipath profiles (e.g., delay and Doppler along each path) from received signals enables many important applications, such as channel prediction and crossband channel estimation (i.e., estimating the channel on a different frequency). The benefit of multipath estimation further increases with mobility since the channel in that case is less stable and more important to track. Yet high-speed mobility poses significant challenges to multipath estimation. In this paper, instead of using time-frequency domain channel representation, we leverage the delay-Doppler domain representation to accurately extract and predict multipath properties. Specifically, we use impulses in the delay-Doppler domain as pilots to estimate the multipath parameters and apply the multipath information to predicting wireless channels as an example application. Our design rationale is that mobility is more predictable than the wireless channel since mobility has inertial while the wireless channel is the outcome of a complicated interaction between mobility, multipath, and noise. We evaluate our approach via both acoustic and RF experiments, including vehicular experiments using USRP. Our results show that the estimated multipath matches the ground truth, and the resulting channel prediction is more accurate than the traditional channel prediction schemes.

CCS CONCEPTS

 Networks → Mobile networks; Wireless access networks; Network protocol design; Network reliability.

ACM Reference Format:

Ghufran Baig¹, Changhan Ge¹, Lili Qiu^{1,4}, Yuanjie Li², Wangyang Li¹, Wei Sun¹, Jian He¹, Zhehui Zhang³, Songwu Lu³. 2022. Extracting and Predicting Multipath Profiles under High Mobility. In *The Twenty-third International Symposium on Theory, Algorithmic Foundations, and Protocol Design for Mobile Networks and Mobile Computing (MobiHoc '22), October 17–20, 2022, Seoul, Republic of Korea.* ACM, New York, NY, USA, 10 pages. https://doi.org/10.1145/3492866.3549710

1 INTRODUCTION

Wireless signals from the transmitter traverse multiple paths (e.g., direct, reflected, refracted paths) and combine at the receiver. The

Permission to make digital or hard copies of all or part of this work for personal or classroom use is granted without fee provided that copies are not made or distributed for profit or commercial advantage and that copies bear this notice and the full citation on the first page. Copyrights for components of this work owned by others than ACM must be honored. Abstracting with credit is permitted. To copy otherwise, or republish, to post on servers or to redistribute to lists, requires prior specific permission and/or a fee. Request permissions from permissions@acm.org.

MobiHoc '22, October 17–20, 2022, Seoul, Republic of Korea

© 2022 Association for Computing Machinery. ACM ISBN 978-1-4503-9165-8/22/10...\$15.00 https://doi.org/10.1145/3492866.3549710 multipath profiles contain important information about the physical propagation paths (*e.g.*, delay and velocity), enabling many applications, such as motion tracking, environment sensing, channel prediction, crossband channel estimation, and beamforming. Hence, there have been several works on estimating multipath profiles based on wireless signals (*e.g.*, [16, 19, 39]). However, the existing works focus on low or no mobility scenarios. Estimating multipath profiles under high mobility arising from vehicles, high-speed rails, drones, or satellites, poses significant challenges.

Yet getting multipath parameters under high mobility is especially useful. For example, it allows a cellular base station to track vehicular motion and its environment without feedback. It can also apply the sensed information to select a data rate or optimize beamforming. [2] shows that multipath information helps improve beamforming performance. Moreover, it can also use the multipath information to estimate the channel on another frequency (*e.g.*, use the uplink channel to estimate the downlink channel) since the underlying propagation paths are the same [39].

In addition, by extracting the current multipath information, we can predict the multipath in the future and then map them to the wireless channel. It is promising since delay and doppler correspond to physical movement and are likely to be more predictable than the wireless channel, which is the outcome of complicated interactions between mobility, multipath, interference, and noise.

Hence, we develop a novel algorithm to estimate and predict the multipath profiles and apply it to channel prediction as an example application. Instead of using the common time-frequency domain channel representation, we leverage the delay-Doppler domain representation for multipath estimation since it can effectively separate paths with different delay or Doppler. Below we first overview the background and existing work, then introduce our approach.

Delay-Doppler channel representation: Wireless channels can be represented in three interchangeable domains: time, frequency, or delay-Doppler. The delay-Doppler channel representation is:

$$h(\tau, \nu) = \sum_{i=1}^{P} a_i \delta(\tau - \tau_i) \delta(\nu - \nu_i), \tag{1}$$

where $h(\tau, \nu)$ is the channel parameterized by the delay τ and Doppler ν , P is the number of propagation paths, $\delta()$ is the Dirac delta function, and a_i , τ_i and v_i are the gain, delay, and Doppler shift associated with the i-th path, respectively [7]. Fig. 1 shows an example of a delay-Doppler channel of two propagation paths: a static path (Doppler=0) and a moving path (Doppler \neq 0).

Rationale for delay-Doppler representation: Multipath signals may experience different delays and Doppler shifts and interfere with each other at the receiver. In the widely used time domain or frequency domain, all paths are mixed, and the resulting phase and amplitude change with the delay, Doppler, and relative magnitude of these paths. While one can formulate a non-convex optimization

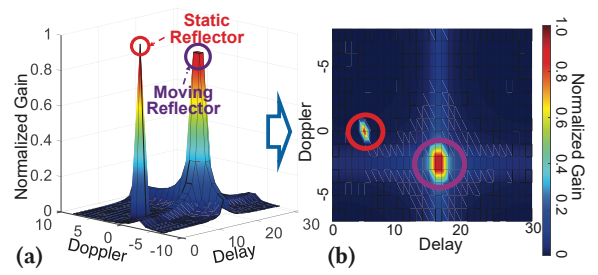


Figure 1: An example delay-Doppler profile. The two peaks in (a) correspond to two reflectors: one is static and one is moving. (b) shows the profile in 2D, where the cross patterns are delay and Doppler spreads.

problem to find the multipath parameters that best fit the measured channel, due to the strong inter-path dependency and the non-convex objective, the problem is fundamentally challenging. While there have been a few works studying this problem, they mostly assume no or low-mobility scenarios and ignore Doppler shift (e.g., [16, 19, 39]) and find the remaining path parameters to best match the measured channel. It is challenging to achieve high accuracy, especially when estimating all multipath parameters (not just the first path). mD-Track [45] uses beamforming to separate the paths spatially and reduce the number of interfering paths. But the beamforming resolution is coarse due to a small number of antennas and large wavelength in sub-6GHz, which significantly limits the effectiveness of spatial separation. When different multipath is not well separated spatially, the estimation error is high, as shown in Section 3.

In comparison, as shown in Fig. 1, the delay-Doppler representation projects signals onto the 2D delay-Doppler plane to separate out paths different in either delay or Doppler. Therefore, only the paths that have similar delay and similar Doppler can interfere, which is much fewer in number. Then instead of solving an optimization problem involving all paths, we only need to solve a much smaller problem involving the interfering paths whose delay and Doppler are both similar, which is more tractable. Moreover, delay and Doppler correspond to physical movement and are more predictable due to inertial, which can help predict channel on a different frequency or at a different time.

Our approach: In this paper, we leverage the delay-Doppler representation to estimate and predict multipath profiles, and demonstrate its utility for channel prediction as an example application.

We first consider estimating multipath profiles based on the measured channel. At first glance, the problem appears simple when paths with different delay or Doppler are fully separated in the delay-Doppler domain, and we can use their positions in the 2D profile to determine their path properties. This method works when we have high SNR and enough separation between the delay or Doppler across different paths. To handle general scenarios, we need to address the following challenges: (i) paths with similar delay and Doppler interfere with each other, and we do not know how many paths interfere; (ii) we may not have enough constraints to uniquely determine each path property; (iii) there is a non-linear relationship between the path properties and the resulting channel, making it hard to find an optimal solution; and (iv) noise can further complicate the issue by introducing false peaks.

To address these challenges, we leverage the sparsity of the multipath and the structure of the channel profile to design an inference algorithm. In particular, we develop a classifier to filter out the false peaks introduced by noise. Then we group nearby peaks into a cluster and infer the multipath profile to match the channel measurement in each cluster. To improve the accuracy and speed, we develop an effective initialization algorithm and iterative method to match the channel measurement.

Then we predict future delay-Doppler based on the current multipath estimates. We match the propagation paths from one time window to the next, and then leverage the temporal relationship between the delay-Doppler of the paths in adjacent time windows. Finally, we map the predicted multipath to the channel estimate.

Our work is partially inspired by the recent orthogonal time-frequency space modulation (OTFS) but differs from it in that we (i) extract multipath properties from the channel estimate, and (ii) predict the future multipath properties and resulting channel. To ease the deployment, unlike OTFS, our approach does not modify the data modulation. Instead, we introduce our own pilot symbols (e.g., 1.5% overhead in our evaluation, lower than LTE pilot overhead) to extract the delay-Doppler of the wireless channel to help channel prediction. In this way, we can support different data modulations, including OFDM, OFDMA, and OTFS, to preserve backward compatibility and maximize flexibility.

We experimentally validate our multipath estimation and channel prediction. We use acoustic signals to complement our RF experiments since acoustic signals propagate slower and induce noticeable Doppler shift at a lower speed, making it easy for experiments. Our results show that it can estimate the multipath delay and Doppler under line-of-sight (LoS) and non-line-of-sight (NLoS).

We further evaluate RF signals using Wireless Insite [14], a commercial 3D ray-tracer widely used by the community [15, 18, 41], and vehicular experiments. Our method yields accurate estimation of both delay and Doppler. Using the estimated multipath, our approach achieves a <7% channel prediction error, whereas the traditional method incurs 60% error. Moreover, our USRP implementation shows our improved channel prediction significantly reduces the BER. Compared to the default channel prediction, our scheme improves BER by up to 10x for SNR of 5 dB. For higher modulation, the improvement is 100x for SNR of 10 dB and up to 1000x for an SNR of 15 dB. We further conduct vehicular experiments to validate the accuracy of our delay-Doppler estimation.

To summarize, our major contributions are as follows:

- 1. We extract multipath properties based on the delay-Doppler representation of wireless channel (Section 2.2).
- 2. We leverage the estimated multipath properties to predict the future multipath and resulting channel (Section 2.3).
- 3. We use acoustic experiments, Wireless Insite simulation, USRP emulation, and vehicular experiments to demonstrate the potential of our approach (Section 3).

2 CHANNEL PREDICTION

Instead of predicting the channel in the classical time-frequency domain, we estimate the multipath properties based on the delay-Doppler representation of wireless channel, predict these path properties, and use the path prediction to forecast the channel. Our key insight is that the client's mobility trajectory is much easier to

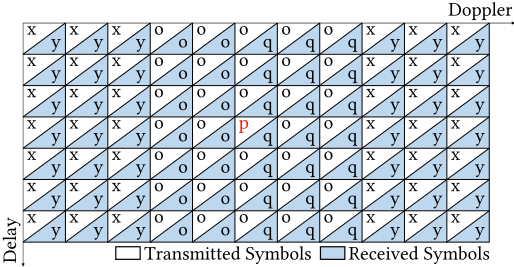


Figure 2: Transmitted/received symbols in the delay-Doppler domain, where x are TX data symbols, p are pilot symbols, o are guard symbols, y are RX data symbols, q are RX pilot symbols for channel estimation.

predict (due to inertia) than the time-frequency channel. Therefore, we decompose the complicated channel prediction into four subproblems: (i) measure channel (§2.1), (ii) extract delay-Doppler of the current paths (§2.2), (iii) predict delay-Doppler of the future paths (§2.3), and (iv) map the future delay-Doppler to the future channel estimation. Among them, (iv) can be achieved by applying Equation 1. So we focus on the first three steps.

2.1 Delay-Doppler Channel Measurement

We consider a classical time-frequency plane (e.g., OFDM and OFDMA) with $N \times M$ grids, where each grid spans T seconds in time and Δf Hz in frequency. A frame is transmitted over NT seconds and $M\Delta f$ Hz. Following [12], the corresponding delay-Doppler plane is divided into $N \times M$ grids where grid (k, l) denotes $(k/(NT), l/(M\delta f))$ and each grid spans $1/(M\delta f)$ and 1/(NT) along the delay and Doppler axes, respectively.

To ease deployment, we keep the existing preamble for synchronization as usual, and introduce our own pilot symbols to estimate the channel in the delay-Doppler domain. The pilot has only 1.5% overhead in our evaluation, which is lower than LTE on 20 MHz and even lower on a wider band. We use the reference signal described in [31] as our pilot. It places a single pilot symbol in the delay-Doppler grid at the k_p -th Doppler tap and the l_p -th delay tap and no symbols at the other taps as guard symbols as shown in Fig. 2. Essentially, the reference signal x is defined as

$$x(k,l) = \begin{cases} 1, & k = k_p, l = l_p \\ 0, & \text{Otherwise} \end{cases}$$
 The received symbol is shifted accord-

ing to the delay and Doppler of the paths that the signal traverses. The amount of the shifts in the delay and Doppler axes reflect the delay and Doppler of the paths the signal has traversed, respectively.

Such pilots can be transmitted on either a data channel or control channel. Sending on the control channel may make it easier to deploy incrementally. Since we estimate the physical path properties, they are invariant to the data modulation scheme and the frequency used for transmission. Therefore, our approach can be applied to predict the channel for OFDM, OFDMA, and OTFS. It can also be used to estimate channel in other frequencies, which has been studied in [6, 21, 39], but these works do not study the channel prediction problem.

2.2 Extracting Multipath Parameters

To extract the delay-Doppler profile from the channel measurement, we first make a few observations about the channel in the delay-Doppler domain. Then we elaborate our solution based on them.

2.2.1 Observations. We have the following observations.

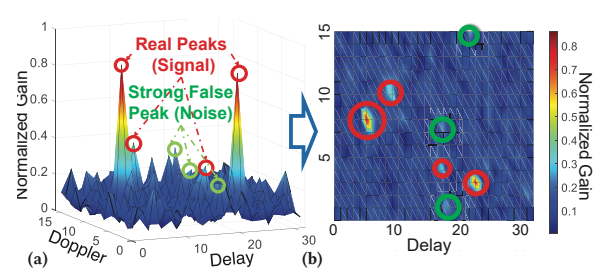


Figure 3: Noise introduces numerous false peaks.

Spread in measured Delay-Doppler channel: Suppose the reference signal x goes through a channel with a single path with delay (τ) , Doppler (v), and attenuation (h). If $\frac{\tau}{M\Delta f}$ and $\frac{v}{NT}$ are integers, the received signal y should have the pilot symbol shifted by $\frac{\tau}{M\Delta f}$ along the delay axis and $\frac{v}{NT}$ along the Doppler axis.

$$y(k,l) = \begin{cases} h, & k = k_p + \frac{v}{NT}, l = l_p + \frac{\tau}{M\Delta f} \\ 0, & \text{Otherwise} \end{cases}$$
 (2)

However, the situation gets complicated when τ and v are not exactly integer multiples of tap resolutions such that

$$\tau = (\alpha + a) \frac{1}{M\Delta f}, \ \alpha \in \mathbb{Z}, \ -1/2 < a < 1/2,$$
$$v = (\beta + b) \frac{1}{NT}, \ \beta \in \mathbb{Z}, \ -1/2 < b < 1/2.$$

In this case, [34] shows that the received signal y can be expressed as follow

$$y[k,l] = \sum_{q=0}^{M-1} \sum_{r=1}^{N-1} \left(\frac{e^{j2\pi(-q-a)} - 1}{Me^{j\frac{2\pi}{M}(-q-a)} - M} \right) \left(\frac{e^{-j2\pi(-r-b)} - 1}{Me^{-j\frac{2\pi}{N}(-r-b)} - N} \right)$$

$$he^{-j2\pi\tau v} x[(k-\beta+r)_N, (l-\alpha+q)_M]$$
(3)

where x is the transmitted signal, A_N is A mod N, α and β are integer parts of the delay and Doppler shift, respectively, q and r denote the delay and Doppler spread, respectively. It has $x[(k-\beta+r)_N,(l-\alpha+q)_M]$ since the received signals in the delay-Doppler domain is a 2D periodic convolution of the transmit signal with the delay-Doppler channel.

Hence, in the case of fractional delay or Doppler, the received pilot symbol will spread across multiple taps. It allows us to estimate the fractional part based on the spread in each direction. This works well under a single path and high SNR. However, noise and multipath make it challenging to extract the precise delay and Doppler based on the channel measurement.

Multipath: Multipath propagation is common in real-world wireless communication. If multiple paths have large enough separation in either delay or Doppler, these paths result in separate peaks in the received frame. We can determine the delay and Doppler associated with each peak independently. When the multiple paths are close to each other in both delay and Doppler, they interfere and change the resulting peak position and spread. We need to jointly estimate all paths contributing to the peak in such cases.

Noise: So far, we assume the peaks are due to signals arriving from one or more propagation paths. In practice, the wireless channel can be noisy, complicating the estimation. Fig. 3 plots an example delay Doppler profile. There are four real peaks and many noisy peaks. Some noisy peaks are higher than one of the real peaks.

2.2.2 Problem Formulation. Suppose there are P paths defined as $\mathbb{P} = \{(\tau_1, v_1, a_1), ..., (\tau_P, v_P, a_P)\}$, where (τ_i, v_i, a_i) denotes the delay, Doppler, and attenuation of path i. Here $\tau_i = (\alpha_i + a_i) \frac{1}{M\Delta f}$ and $v_i = (\beta_i + b_i) \frac{1}{NT}$ where α and β are integers and a and b are fractions. The resulting channel can be derived as follow:

$$\begin{split} y[k,l] &= \sum_{i=1}^{P} \sum_{q=0}^{M-1} \sum_{r=1}^{N-1} \left(\frac{e^{j2\pi(-q-a_i)}-1}{Me^{j\frac{2\pi}{M}(-q-a_i)}-M} \right) \left(\frac{e^{-j2\pi(-r-b_i)}-1}{Me^{-j\frac{2\pi}{N}(-r-b_i)}-N} \right) \\ h_i e^{-j2\pi\tau_i v_i} x[(k-\beta_i+r)_N, (l-\alpha_i+q)_M] \end{split} \tag{4}$$

Our goal is to estimate the multipath parameters such that they can match with the measured channel. That is, we solve the following optimization problem to minimize the difference between the measured and estimated channel.

$$\underset{(\tau_{l}, \nu_{l}, h_{l}) \in \mathbb{P}}{\operatorname{arg min}} \sum_{k=k_{\min}}^{k_{\max}} \sum_{l=l_{\min}}^{l_{\max}} |y_{\text{meas}}[k, l] - y[k, l]|$$
 (5)

There are several challenges in the path estimation: (i) The function is non-convex. There can be lots of sub-optimal solutions. It is expensive to achieve global optimal. (ii) The problem may be under-constrained and do not have a unique solution. There are 3 unknowns associated with each path: delay, Doppler, amplitude. So 3K unknowns for K paths. The number of constraints is the number of affected taps, which can be smaller than the number of unknowns. (iii) The number of underlying paths is unknown, which means we do not know the number of unknowns. (iv) Noise complicates the path estimation by introducing noisy peaks.

2.2.3 Our Approach. We develop a novel path estimation approach. It leverages both domain knowledge and machine learning to maximize accuracy. From the above observations, multipath would interfere if they have similar delay and Doppler. The paths with large separation in the delay and Doppler will result in separate peaks and can be estimated independently. Therefore, we first detect the grid locations that have some signal energy and separate them from the grid locations that have only noise. Our signal detection should be robust against noise. Then we cluster the grid locations with signal based on their positions in the delay-Doppler profile. A major benefit of estimating the multipath in the delay-Doppler domain is the ability to separate paths with either different delay or Doppler to only solve an optimization problem for each cluster, which involves fewer variables, thereby improving accuracy and speed. We further leverage our domain knowledge in initialization to enhance the performance. Below we elaborate each step.

To improve the signal detection, we observe that taps with the actual signal tend to have both high magnitude and spatial locality since both fractional delay and fractional Doppler result in multiple nearby taps having the signal energy. This observation motivates us to develop a neural network (NN)-based classifier to determine whether a tap has a peak due to the real signal.

Our classifier takes the concatenated amplitude and phase of the complex signal in the delay-Doppler domain as the input and outputs whether the tap contains real signal. Intuitively, it uses the training data generated using simulation based on Equation (3) and model the spread of signal due to fractional delay and fractional Doppler. We vary the SNR from -5 dB to 10 dB. It is easy to generate the label since we can inject multipath and know which taps each

path should affect. The original delay-Doppler profile is a $N\times M$ matrix. To make the classifier easy to train, we limit the input and output size by taking only a portion of this matrix as the input and outputting whether the center tap in the grid has energy from the real signal. This is reasonable since each cluster spans only a small number of taps. We can apply the classifier to each tap by taking a sub-matrix centered at the corresponding tap. For a tap on the boundary of the matrix, we can construct its matrix by wrapping around. We generate the training data by simulating different overlapping multipath patterns and varying the SNR from -5 dB to 10 dB. The label for each data point is determined based on the injected multipath.

Our neural network consists of one hidden layer with 50 neurons followed by ReLu non-linearity and one output layer with Softmax activation function. The output is a one-hot encoded vector of size 2, whose elements denote the probabilities that the center of the grid contains only the noise or signal. We determine whether the center grid has signal based on which probability is higher during inference. Since there are many more taps with only noise than with the signal, to avoid bias, we ensure the numbers of taps with and without a peak due to the signal are similar in the training data. During testing, we apply the neural network to each tap in the grid using a 5x5 grid centered at that tap to determine if it has signal. Cluster peaks: Once grid locations with peaks due to the signal are detected, we cluster them spatially and infer the multipath properties for each cluster. Clustering is motivated by the observation that well-separated peaks are caused by the paths with different delay or Doppler and do not interfere with each other. Therefore, the peaks belonging to different clusters are independent. We group peaks within 2 taps together into the same cluster and infer multipath properties to match the measured channel in each cluster. Clustering reduces the number of the multipath parameters, and improves both efficiency and accuracy.

Estimate the delay-Doppler: Next, we estimate the delay-Doppler for each cluster. Our goal is to determine the multipath parameters so that the resulting channel best matches with the measured one.

This is a non-convex optimization problem. We use the well known interior-point method to solve this problem. However, since the optimization function is non-convex, the optimization can converge to a non-optimal local minimum. Therefore, a good initialization is important for both the speed and quality of the solution.

We initialize the solution for every cluster in the following way. Due to temporal locality, the multipath parameters corresponding to a cluster remain stable for a while. Therefore, we first compute the channel in the cluster using the previous multipath parameters and Equation 4. Suppose the resulting delay-Doppler channel for the cluster is similar to the current channel (i.e., the difference is within 15% of the current channel, where the delay-Doppler channel is represented as a matrix for the cluster and the difference between the two channels C_1 and C_2 is quantified as $norm(C_1 - C_2)/norm(C_2)$). In that case, we use the previous multipath parameters as the initial solution for that cluster. Otherwise, we derive the initial solution based on the current peaks' positions in the delay-Doppler grid since the peaks are usually close to the actual delay and Doppler. We detect the peaks in the measured channel and use the peak position for initialization. This is important especially in cases where multipath changes significantly between two measurements. We

use the number of detected peaks to initialize the number of paths in a cluster and use the peak positions to initialize the paths' parameters; we then iteratively add more paths to improve the fit with the measurement. This is a reasonable approach since the number of peaks provides a lower bound on the number of multipath due to peak merging. In this way, we can handle large changes in multipath parameters and avoid error propagation.

Initializing using the previous multipath parameters or the current peak positions is likely to yield a close-to-optimal solution, speed up the convergence, and improve the solution quality. However, they are not optimal. Therefore we feed the initial solution to the optimization algorithm (e.g., interior-point method in Matlab). If the fitting error is less than 2x the noise estimate, we use the solution as the final estimate (The noise is estimated as the average power in the grid locations where no peak is detected). Otherwise, we add a new path. In the latter case, we initialize the multipath properties to the solution from the previous iteration. We initialize the new path by canceling the existing path and detecting the peak in the remaining signal. We then feed the new initialization to the optimizer and iterate until the fitting error is small enough (e.g., less than 2x of the noise estimate). Alg. 1 shows our pseudo code.

Note that our goal is to predict the channel in the future accurately. Therefore it is robust to occasionally miss or add a small number of paths if their magnitude is small. These paths do not significantly affect the channel estimation and prediction. This will likely hold since we try to minimize the fitting error with the measured channel.

Algorithm 1: Delay-Doppler estimation pseudocode

Computation time: Initializing using the multipath parameters from the previous interval takes within 4 ms, which is fast enough to support real-time decoding since a single frame lasts 10 msec in LTE. We use the previous estimation for initialization when no new path is outside the previous clusters. Initializing using the previous estimates works for at least 92% of time and during this time the prediction error is within 6%. Our algorithm automatically detects initializing using a previous estimate yields a large difference from the measured channel and then initializes from scratch. To support real-time data decoding, we initialize using the previous estimates (since it is much faster) and in parallel also initialize from scratch so that we can later obtain more accurate initialization to improve the channel prediction. We call this phase as catch up phase. In both cases, we use optimization to further improve the solution. We find the error during this catch up phase is 25% on average, still much lower than the baseline: 40% error. The duration of the catch up phase varies depending on the number of multipath that merge into a single peak: 9, 18, and 32 ms for 2, 3, 4 paths, respectively. These numbers show that our approach is practical and can support real-time decoding.

2.3 Predict Future Paths in Mobility

The next step is to predict how the channel changes before the next channel measurement is taken. While channel prediction has been widely studied, the existing works directly use the previous channel as the input for prediction. It is hard for this type of prediction schemes to achieve high accuracy due to multipath. Instead of predicting the channel directly, we predict the delay Doppler and map them to the channel. This problem is related to mobility prediction but differs from the existing mobility prediction in that our work predicts the delay-Doppler of all multipath whereas the existing mobility work focuses on predicting the mobility of a single target. Therefore, we design a new algorithm for this purpose.

Matching paths over time: We apply our algorithm to get the delay-Doppler of paths over time. We expect the delay and Doppler of the same propagation path to be strongly correlated. Therefore we should pair the delay-Doppler of the paths between two consecutive intervals (*e.g.*, determine which path in the current interval corresponds to a given path in the previous interval). We leverage the temporal locality to determine the mapping.

This problem can be formulated as a matching problem. We define a bipartite graph where the vertices on the left denote the paths in the previous interval and the vertices on the right denote the paths in the next interval and the weights of their edges reflect the difference between the delay-Doppler properties of the corresponding paths. We use Euclidean distance in the delay-Doppler profile as the weight between two paths. Namely, $\sqrt{(d_i^{t1}-d_j^{t2})^2+(v_i^{t1}-v_j^{t2})^2}$, where d_i^{t1} and v_i^{t1} denote the delay and Doppler of path i at t1, respectively, and similarly define d_j^{t2} and v_j^{t2} . Our goal is to find a minimum weighted matching that minimizes the difference between the paths in two consecutive intervals. We use Munkres algorithm [26] to solve the matching problem. Its complexity is $O(n^3)$. This is affordable since the number of paths n is usually small (e.g., within 8).

Matching helps facilitate the path prediction. The above matching works well when the same set of paths are present in both intervals. Now we consider the set of paths changes between the two intervals. There are three cases: (i) old paths disappear, (ii) new paths emerge, (iii) old paths disappear and new paths appear at the same time. In (i), we no longer need to predict the old paths and use the delay and Doppler of the remaining paths to compute the new channel. In (ii), the new paths are unlikely to be matched with any of the old paths and we just use the current delay Doppler of the new paths to predict their future delay Doppler. In (iii), the main concern is that new paths may match with old paths and pollute the prediction process. To prevent that, we consider the matching is good only if the difference between the matched path is small enough. If so, the path is most likely to be the same across the two intervals and we can use the path properties in both intervals for prediction. Otherwise, it means the current path is likely to be new and we can only use the latest path properties for prediction.

Predicting Path Properties: Once we match the paths across two intervals, we will make path prediction for the next interval. We try both exponential weighted moving average (EWMA) and Holt-Winters (HW) [1]. EWMA predicts the future quantity as $x_{est} = \alpha x_{est} + (1 - \alpha)x$, where x is the current sample and x_{est} is the predicted value, and α is the weight for x_{est} and between 0 and

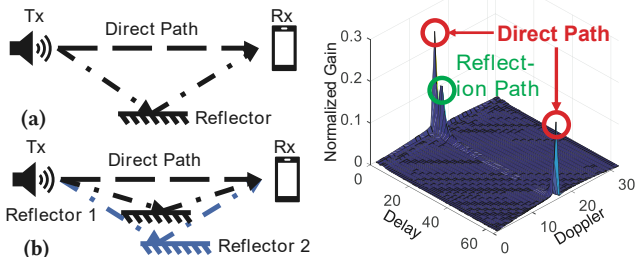


Figure 4: Acoustic experi-Figure 5: Acoustic delayment.

Doppler profile.

1. Holt Winter improves over EWMA by decomposing the predicted value into two components: fluctuation a(i) and trend b(i): y(i+1) = a(i) + b(i) where $a(i) = \alpha \times y(i) + (1-\alpha) \times (a(i-1) + b(i-1))$ and $b(i) = \beta \times (a(i) - a(i-1)) + (1-\beta) \times b(i-1)$. Our evaluation shows that both work pretty well and Holt Winter slightly out-performs EWMA since it can predict the trend in the data. So we use Holt Winter in our evaluation and set $\alpha = \beta = 0.7$.

3 EVALUATION

We first evaluate using acoustic signals since its Doppler shift is large even at a lower speed due to its slower propagation speed, making it easier for experiments and getting the ground truth. Next, we use a combination of Wireless Insite and vehicular experiments using USRP to evaluate our approach for RF signals.

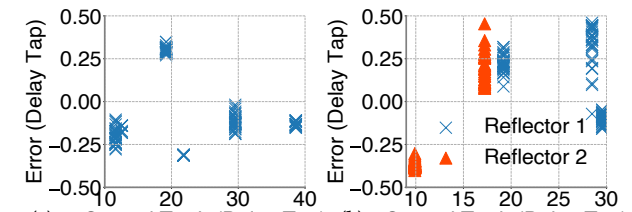
3.1 Acoustic Micro-benchmark

Acoustic signals are attractive to use for validation since it has better distance and Doppler resolution. We use 14-22 KHz acoustic channel, 8KHz bandwidth, 250 ms pilot spanning 64×32 grid. Therefore, each distance tap is $\frac{c}{B}=4.25$ cm and Doppler tap is $\frac{B}{MN}=3.91$ Hz corresponding to 7.44 cm/s, where c is the speed of sound and B is bandwidth. It allows us to differentiate between slow movement, which is easy for conducting controlled experiments.

We first evaluate how accurately our approach estimates the delay-Doppler profile by comparing the ground truth distance and velocity. We run our tests in an anechoic chamber using the setup shown in Fig.4. For validation, we generate acoustic signals with a preamble followed by multiple pilots similar to Fig.2. We play signals through a speaker. We use a smartphone as a receiver to record the received signals. The receiver first runs correlation with the preamble to detect the start of the transmission and then estimates the delay and Doppler using the approach described in Sec.2. After synchronization, the delay estimated using the subsequent pilots reflects the delay change since the preamble.

Delay-Doppler profile: Fig. 5 plots an example delay-Doppler profile after processing the received acoustic signals. After synchronization, the shortest path is shifted to the tap 0. The tap at the largest delay also corresponds to the direct path due to wrap around. The reflection path has slightly larger delay and weaker signal strength. The difference between the delay of the direct path and reflection path matches with the ground truth in our setup.

Distance estimation: We add a reflector as shown in Fig. 4(a). We fix the positions of the transmitter and receiver, and move the reflector around. Our analysis of received signal shows two distinct peaks corresponding to the direct path and reflected path. Fig. 6(a) plots the delay estimation error of the reflected path as we move the reflector from 12 taps to 29 taps. The error is within 0.4 tap, which is quite small. Then we add another reflector as shown in



(a) Ground Truth (Delay Tap) (b) Ground Truth (Delay Tap) Figure 6: Delay estimation error in LoS acoustic experiments: (a) single reflector and (b) two reflectors.

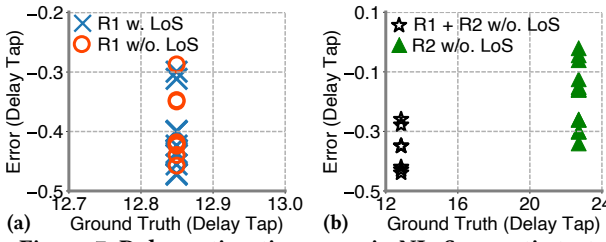


Figure 7: Delay estimation error in NLoS acoustic tests

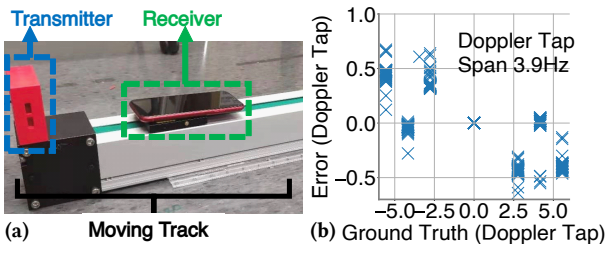


Figure 8: Doppler estimation in acoustic experiments.

Fig. 4(b). Our path estimation automatically determines there are 3 paths and derives their corresponding delay and Doppler. Fig. 6(b) shows the distance estimation error of the two reflection paths. They remain small – within 0.5 tap.

We further evaluate under NLoS scenarios. We place a phone and speaker with LoS and add a reflector. After synchronization, the receiver shifts the LoS path to tap 0 and accurately estimates the distance difference between the reflected and direct paths. As shown in Fig. 7(a), the estimation error is within 0.5 delay tap in blue. Then we block the LoS path. The receiver continues to accurately estimate the delay of the NLoS path within an error of 0.5 delay tap as shown in red in Fig. 7(a). Next we add a second reflector. Fig. 7(b) shows our estimated delay of both reflection paths have low errors: within 0.5 and 0.35 taps for the two reflectors. These results demonstrate the feasibility of our delay estimation in NLoS.

Doppler estimation: Next, we evaluate the performance of Doppler estimation. We put our transmitter on a moving track and put the receiver on a table as shown in Fig. 8(a). We control the speed of the moving track from 20 cm/s to 40 cm/s so that we know the ground truth velocity. As shown in Fig. 8(b), our Doppler estimation error is also small, ranging between 0 - 0.75 tap. Note that the acoustic signals occupy 14-22 kHz, which means the Doppler shift in the 8 kHz band varies with the frequency. This is already visible in the movement speed we use and contributes to our estimation error. Further increasing the moving speed will introduce more peaks in the Doppler axis due to the frequency-dependent Doppler shift, making it hard to visualize the results. Therefore, we limit our speed to 40 cm/s. This is a unique problem in acoustic signals due

to their low frequency. For RF signals, the entire 20 MHz channel sees almost the same Doppler shift due to its higher frequency (*e.g.*, above 2 GHz), and hence has even lower estimation errors.

3.2 Wireless Insite Based Evaluation

Next we evaluate our approach using Wireless Insite.

3.2.1 Evaluation Methodology. Transmission signals: RF signals propagate much faster than acoustic signals, which leads to more coarse resolutions. Our default configuration uses 20 MHz bandwidth and sampling frequency, 512×256 grid for a frame, and a 32×64 sub-grid for a pilot. This yields a delay resolution of $\frac{c}{B} = 15m$, and Doppler resolution of $\frac{B}{MN} = 152.5$ Hz. This Doppler resolution corresponds to a speed of 21.5 m/s for 2.125 GHz, 1.6 m/s for 28 GHz, and 0.76 m/s for 60 GHz. We use USPS for our vehicular experiments. Meanwhile, we also conduct an extensive evaluation using Wireless Insite. Our pilot overhead is $\frac{32 \times 64}{512 \times 256} = 1.56\%$, which is lower than LTE pilot overhead of 4.7%. Moreover, since we estimate the physical path properties and no longer need to send pilots for different frequencies, our pilot overhead is even lower than wideband LTE.

Multipath in 3D environment: To generate realistic traces, we recreate 3D real-world models of our test fields and feed them to Wireless Insite, which ray-traces RF signal reflection, penetration, and diffraction under the LTE frequency band. We use the parameters from our driving traces to make our evaluation as realistic as possible. We pick a $2.6 \times 1.8 \text{ km}^2$ satellite city for our measurement and simulation, which includes campus, downtown urban canyon, suburban, and pure highway. The measurements cover diverse road types, including highway, railway, primary, secondary, tertiary roads, and parking lots. The reconstruction of 3D model follows a Geographic Information System (GIS) based pipeline [41]. We use bounding longitude and latitude of these areas in blender-osm [10] to fetch the terrain and building information from OpenStreetMap [9]. Then the Blender [11] graphics software renders the 3D models, colors and splits them based on material texture. Finally, we put all 3D elements together in Wireless Insite and assign dielectric parameters to each surface according to the segmentation. The detailed material settings are from ITU [37, 38] and online material property database [35, 36].

Mobility Trace: We record driving trajectories by logging GPS locations and inertial measurement unit (IMU) readings. Our drives last for 15-30 minutes. We run *Wireless Insite* by setting measured GPS coordinates as the receiver locations and overlaying them onto the 3D models as shown in Fig. 9 (c). In addition, we collect the cell tower IDs using *MobileInsight* [22] during our drives. We obtain the GPS coordinates, transmission power, operational frequency of LTE cell towers from *OpenCelliD* database [20].

Validation: We measure the received signal strength (RSS) from the cell towers roughly every 100 msec using Mobile Insight. We use these measurements to validate the multipath traces from Wireless Insite. Since we do not know the directionality of eNB antennas, we use the omnidirectional antenna and assign the transmit power of every base station such that the RSS in Wireless Insite is equal to the first measured RSS from that base station. For every TX and RX location, we generate multipath by ray tracing in the 3D environment and get the ToF, Doppler, AoA/AoD, and received power of every path. We only use the paths whose received power is

within 20 dB of the maximum for our multipath trace. It also outputs the signal strength of the received signal at every RX location. We compare the RSS from *Wireless Insite* with the RSS measurements from *Mobile Insight*. As shown in Fig. 9, they match quite well, indicating that our methodology generates realistic traces.

3.2.2 Performance Results. We evaluate each component in our approach, which includes peak detection, multipath estimation, channel prediction, and data decoding.

Peak Detection: We compare the accuracy of our peak classifier and threshold based peak detection under varying SNRs (-5~0dB). We use recall and precision to quantify the accuracy. Recall is the ratio between the number of detected real peaks and the number of real peaks, while precision defines the ratio between the number of detected real peaks.

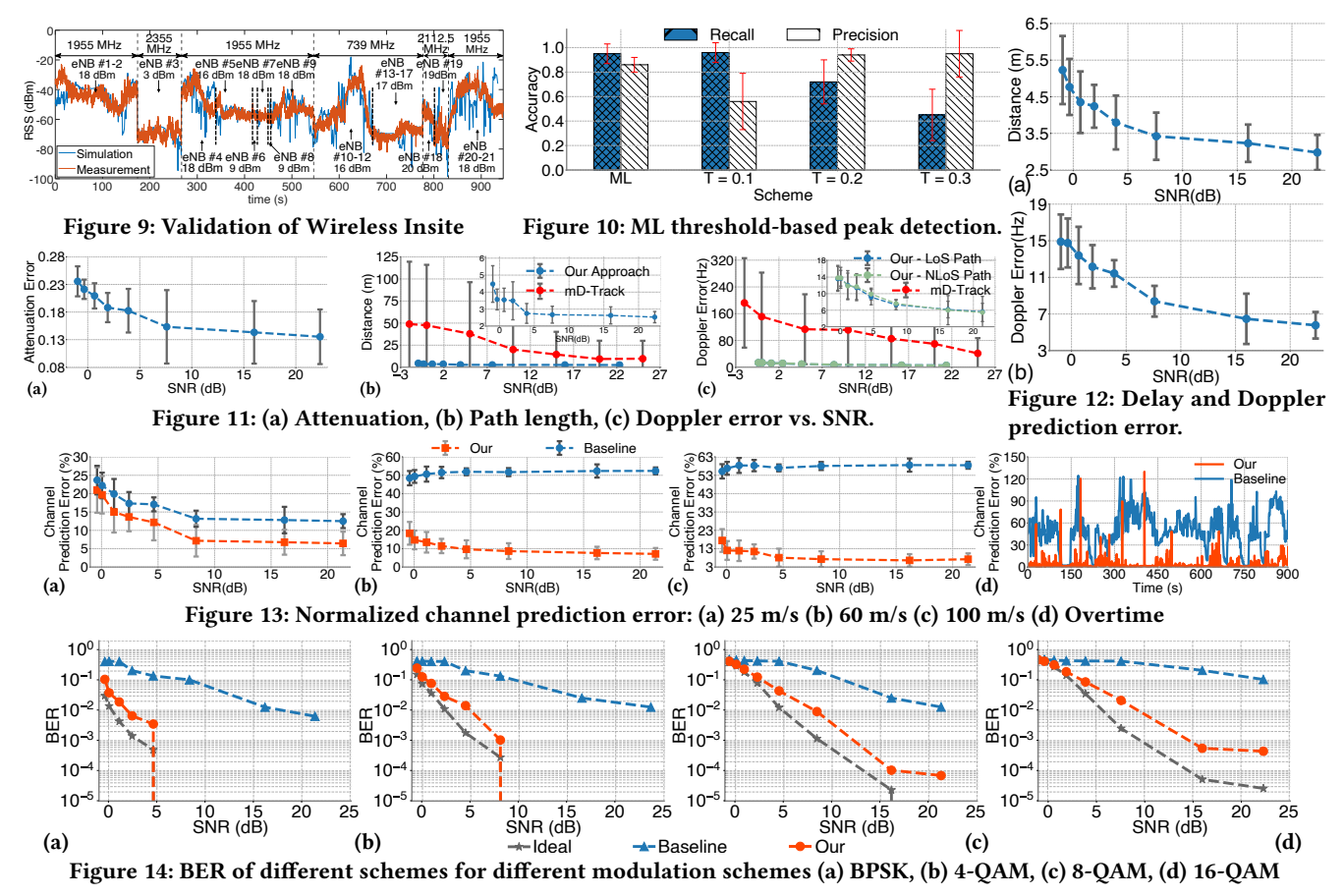
As shown in Fig. 10, our ML-based classifier can achieve both high recall and precision: 0.95 and 0.86, respectively. It achieves higher accuracy because it uses both peak magnitude in the current tap and shape of nearby taps for peak detection. In comparison, the threshold based scheme has either low recall or low precision. When the threshold is low (e.g., 0.1), the threshold based scheme has high recall: 0.96 but low precision: 0.56. Increasing the threshold to 0.3 increases the precision to 0.95 while reducing the recall to 0.45. A low threshold incurs low precision because it considers many noisy peaks as real peaks. A high threshold results in low recall because it misses many real peaks. It is difficult to find a threshold to achieve both high recall and high precision.

3.2.3 Multipath Estimation. Next we evaluate how accurate our algorithm estimates different multipath parameters and how the estimation affects the channel prediction.

Attenuation estimation: Fig. 11(a) shows the estimation error of the attenuation coefficient for each path relative to the coefficient of direct path in multipath environments as described above. Our results show the normalized error for the attenuation is around 20% for 0dB SNR and within 15% for 10 dB SNR and above.

Delay estimation: As shown in Fig. 11(b), even for a low SNR of 0dB, our delay estimation error is within 3.5m. For a higher SNR, our error is within 2.5m, which is 2% of average path length in our traces. In contrast, the mD-Track using 4 antennas yields a large delay estimation error. Only when the SNR is above 20 dB, the average path length estimation error is lower than 10m. In general, the delay estimation error in mD-Track is 5× to 10× higher than our error. This is not surprising since the delay-Doppler channel representation allows us to reduce the number of interfering paths and make the optimization problem smaller and easier to solve while mD-track cannot spatially separate out the multipath based on angle of arrival (AoA) due to a small number of antennas.

Doppler estimation: Fig. 11(c) compares our Doppler estimation with mD-Track for the LoS and NLoS paths. Our approach has Doppler estimation error around 12 Hz for a low SNR of 0dB and within 10 Hz for SNR \geq 5 dB, which is within 2% of average Doppler shift in our traces. Moreover, our estimation error is small for both direct and reflection paths. mD-Track yields a high Doppler estimation error: its Doppler error is 8× to 11× higher than our estimation error since spatially separating the multipath is harder in this case. **Path prediction:** Next we use the estimated path parameters to predict the future parameters for each path. We use Holt-winter algorithm to predict the future parameters based on the current



estimates. Fig. 12 shows that the prediction is accurate even for low SNRs – within 5 m and 15 Hz.

OFDM channel prediction: We predict the OFDM channel based on the predicted multipath parameters. We compare our prediction with the existing work that predicts the channel by interpolating between the two reference blocks on a given subcarrier. The reference blocks are separated by 7 slots as they are in an LTE frame. Fig. 13 shows the average normalized error across all slots in the same subframe and subcarrier where the reference blocks are transmitted. The average error is computed as $|h_{est} - h_{real}|$, where h_{est} and h_{real} denote the estimated and real channel, respectively. Fig. 13 shows that predicting based on interpolation incurs a very high error: 70%, while predicting using multipath parameters is much more accurate. Our scheme reduces the error by up to 10x for a range of SNRs. The speeds in Fig. 13 correspond to 2.125 GHz. If higher frequencies are used, similar benefits will be observed at much lower speeds. For example, 25 m/s, 60 m/s, 100 m/s in 2.125 GHz correspond to 1.9 m/s, 4.6 m/s, 7.6 m/s in 28 GHz, respectively, and correspond to 0.9 m/s, 2.125 m/s, 3.5 m/s in 60 GHz, respectively. Therefore, our approach can benefit transmissions at higher frequencies even more.

We further show how the channel prediction error varies over time as the velocity of the client changes. Fig. 14(d) shows the normalized OFDM channel prediction error using interpolation versus using the predicted multipath parameters. During the intervals

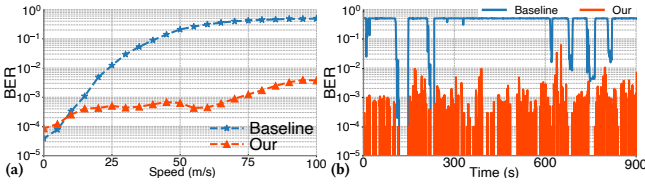


Figure 15: (a) BER vs speed. (b) BER over time

with a low speed, the errors of both schemes are similarly low. In comparison, under high mobility cases (>70m/s), the prediction error of the existing scheme is sometimes over 100%. In comparison, our scheme significantly reduces the prediction error. There are some spikes in our prediction error. This happens when our channel estimation misses some path due to noise. This generally happens when new paths appear in the channel. However, these cases are rare and the error reduces quickly afterwards.

OFDM Data Decoding: We conduct USRP experiments to evaluate our system in high mobility. We use *Wireless Insite* to generate realistic channel under high mobility as mentioned above. We then feed the reference signals similar to the one in Fig. 2 along with the data signals to the generated channel and let a USRP node transmit the resulting RF signals over the air. A USRP receiver processes the received signal to extract the delay and Doppler. We expect the received signal should have similar multipath properties as the synthetic channel since reflectors in the lab environment are not far enough (*i.e.*, > 15 m) to show up in different delay taps. The

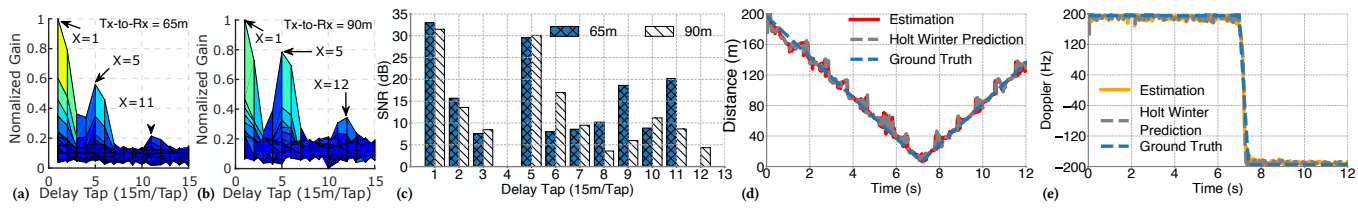


Figure 16: Distance and velocity estimation in vehicular experiments. (a) Static experiment A (65m between Tx and Rx). (b) Static experiment B (90m between Tx and Rx). (c) Ground truth ray-tracing paths binning. (d) Distance estimation in vehicular experiments. (e) Doppler estimation in vehicular experiments.

USRP receiver essentially sees the multipath from the generated channel along with additional noise and interference (if any) from the lab where we run the experiment.

We compare data decoding by predicting the channel using our approach versus interpolation. We compensate the received signal based on the predicted channel before data demodulation.

Fig. 14 compares the BER after applying 1/2 FEC across three schemes: (i) ideal where the channel remains the same, (ii) baseline that uses interpolation and extrapolation to directly estimate the channel, and (iii) our approach that estimates and predicts the multipath properties. We make several observations. First, our approach significantly out-performs the baseline. It is close to the ideal case under low modulation schemes (e.g., BPSK and 4-QAM). Under a high modulation scheme, our approach continues to significantly out-perform the baseline but deviates from the ideal case. This is expected since higher modulations are more sensitive to channel estimation errors. A close look reveals that most channel estimation error arises when we under-estimate or over-estimate the number of multipath. As part of our future work, we will further improve the estimation accuracy. Fig. 15 (a) shows how the BER varies across speeds for a fixed modulation scheme and fixed SNR. It shows that our multipath profile based prediction can achieve much lower BER than the baseline under a high speed.

We further show how the BER varies over time as the velocity of the client changes. Fig. 15 (b) plots the BER of BPSK modulation for baseline and our approach. It shows that the baseline has a very low BER, roughly similar to our scheme, during the intervals with a low speed. This is because the channel is not very dynamic under low mobility and the data symbols see a similar channel as the reference signal. It can be further validated using the results in Fig. 14(d), where it shows that the baseline has a very low prediction error. However, the baseline scheme fails to decode most data under high mobility as the BER is close to 0.5 due to large Doppler shifts. In comparison, our method yields much lower BER at high speed.

3.3 Testbed Experiments

We further conduct testbed experiments. We build our testbed on two Ettus USRP N210, each equipped with a single dipole antenna, serving as TX and RX, respectively. Their clocks are driven by GPS disciplined oscillator (GPSDo). Before experiments, we measure the hardware phase offset on RF chains of USRPs using a cable connection between the TX and RX antenna port. Although the clocks are synchronized, a 0.15~3Hz carrier frequency offset (CFO) still exists. We follow the method in [45] to estimate and compensate CFO in post-processing. Then, the sampling frequency offset (SFO) and symbol timing offset (STO) are calibrated according to [19, 45].

First, we perform static experiments. We separate two USRPs 90 m and 65 m apart. The TX transmit OTFS signal of 16384×32 grids at 1.71 GHz with a 20 MHz bandwidth. This yields 15m delay resolution. The preamble occupies 8192 × 1 sub-grids. Fig. 16(a) and (b) show the delay-Doppler profiles containing 3 peaks for 65m and 90m Tx-Rx separation, respectively. Since the experiment is in LoS, the first peak is the direct path and the synchronization moves the peak to tap 0. To verify the distance estimation, we feed the 3D model of the test field to the Wireless Insite to get the ground-truth multipath in the environment. We bin the ground truth multipath based on their path-length, where each bin is 15m. Fig. 16(c) shows the top few bins. Not all paths in Wireless Insite are visible in real measurements due to noise and interference. But the top three bins from Wireless Insite correspond to the peaks in our delay-Doppler profile in Fig. 16(a) and (b). The delay difference between our estimation and ground truth are 0m for the 2nd and 3rd peaks in the 65m case. The errors are 0m for 2nd peak and 15m for 3rd peak in 90m case due to lower SNR.

Next, we conduct vehicular experiment. We fixed the TX along-side the road and mounted the RX on the vehicle's top. Limited by the transmit power, we set the trace duration to 12s or 320m. The car travels at 26.67 m/s on cruise control, first towards the TX, then passes it and moves away. TX transmits signal at 2.2 GHz. To obtain the ground-truth path length and doppler, we also record the GPS location and trajectory of the TX and RX, respectively. Fig. 16(d) and (e) compare the estimated, predicted, and ground truth delay and Doppler. Our method yields a 6.93% and 4.91% delay and Doppler estimation errors, respectively, and 8.35% and 5.60% delay and Doppler prediction errors, respectively. These results demonstrate the feasibility of our approach in a real environment.

4 RELATED WORK

Channel prediction: Existing works predict the channel in the time-frequency domain (*e.g.*, OFDM). They enhance the prediction accuracy using spatial-temporal correlation [24, 27, 32, 44], machine learning [23], compressive sensing [5, 8], subspace algorithm [3], and external sensor/GPS assistance [13, 30]. High mobility increases the estimation error due to a large Doppler shift.

Cross-band channel estimation:

[39] studies the problem of using OFDM measurement from one frequency to estimate the OFDM channel on another frequency. Since all paths are mixed together in OFDM, the non-linear optimization is much harder to solve. The quality of the solution is sensitive to the initial estimates. Our simulation shows that the path length estimation in [39] has \geq 15 m error even under a high SNR (15 dB). The error increases to 30 m when the SNR reduces to 0 dB. To improve the initial estimation in [39], [6] develops a

machine learning (ML) based algorithm. However, the ML model should be retrained for each frequency. More importantly, [39] and [6] operate in the time-frequency domain, and implicitly assume *static environments* and ignore the Doppler shift. We estimate multipath properties using the delay-Doppler representation for high mobility.

[21] applies singular value decomposition to cross-band channel estimation without extracting multipath parameters. By extracting multipath parameters, we can support applications beyond crossband estimation, including channel prediction, motion tracking, and environment sensing.

Motion sensing: Various motion sensing algorithms and systems have been developed using WiFi [4, 16, 17, 29, 33], mmWave [43, 48], RFID [25, 40], and acoustic signals [28, 42, 46, 47]. Different from motion tracking, which focuses on estimating the first path, we estimate the multipath profile, which is necessary for sensing environments and optimizing wireless communication.

5 CONCLUSION

This paper presents a novel approach that leverages the delay-Doppler representation to estimate and predict the multipath profile. Our results show this approach is promising – its delay estimation error is within 1% under SNR above 10dB and 4% under SNR of -4 dB and the corresponding Doppler estimation error is 0.4% and 2%, respectively. We also show it helps channel prediction. The contribution of our work is beyond a specific algorithm for multipath estimation and prediction, but shows an example application of using the delay-Doppler channel representation in high mobility scenarios. We hope other researchers can develop more applications to benefit from this channel representation.

6 ACKNOWLEDGMENTS

This work is supported in part by NSF Grant CNS-2008824 and CNS-2107037. Yuanjie Li acknowledges the support from the National Natural Science Foundation of China (62132009). We are grateful to anonymous reviewers for their insightful comments.

REFERENCES

- [1] Holt-winters' seasonal method, 2020. https://otexts.com/fpp2/holt-winters.html.
- [2] Two beams are better than one: towards reliable and high throughput mmwave links. In Proc. of SIGCOMM, 2021.
- [3] Ramoni Adeogun. A method for parameter extraction and channel state prediction in mobile-to-mobile wireless channels. 2014.
- [4] Fadel Adib, Zach Kabelac, Dina Katabi, and Rob Miller. WiTrack: motion tracking via radio reflections off the body. In Proc. of NSDI, 2014.
- [5] Waheed U. Bajwa, Jarvis Haupt, Akbar M. Sayeed, and Robert Nowak. Compressed channel sensing: A new approach to estimating sparse multipath channels. In *Proc. of IEEE*, 2010.
- [6] Arjun Bakshi, Yifan Mao, Kannan Srinivasan, and Srinivasan Parthasarathy. Fast and efficient cross band channel prediction using machine learning. In Proc. of MobiCom. 2019.
- [7] Philip Bello. Characterization of randomly time-variant linear channels. IEEE transactions on Communications Systems, 11(4):360–393, 1963.
- [8] Christian R. Berger, Zhaohui Wang, Jianzhong Huang, and Shengli Zhou. Application of compressive sensing to sparse channel estimation. *IEEE Magazine*, 2010.
- [9] Steve Coast. Openstreetmap, 2020.
- [10] Vladimir Elistratov. blender-osm: Openstreetmap and terrain for blender, 2020.
- [11] Blender Foundation. Blender, 2020.
- [12] R. Hadani, S. Rakib, M. Tsatsanis, A. Monk, A. J. Goldsmith, A. F. Molisch, and R. Calderbank. Orthogonal time frequency space modulation. In *Proc. of WCNC*, pages 1–6, March 2017.
- [13] Songtao He, Favyen Bastani, Sofiane Abbar, Mohammad Alizadeh, Hari Balakrishnan, Sanjay Chawla, and Samuel Madden. RoadRunner: Improving the Precision of Road Network Inference from GPS Trajectories. In Proc. of SIGSPATIAL, 2018.

- [14] Remcom Inc. Wireless insite 3d wireless prediction software, 2020.
- [15] Zhiyuan Jiang, Sheng Zhou, Zhisheng Niu, and Cheng Yu. A unified sampling and scheduling approach for status update in multiaccess wireless networks. In Proc. of IEEE INFOCOM, pages 208–216, 2019.
- [16] Kiran Joshi, Dinesh Bharadia, Manikanta Kotaru, and Sachin Katti. Wideo: Fine-grained device-free motion tracing using RF backscatter. In Proc. of NSDI, 2015.
- [17] Bryce Kellogg, Vamsi Talla, and Shyamnath Gollakota. Bringing gesture recognition to all devices. In *Proc. of NSDI*, volume 14, pages 303–316, 2014.
- [18] Aldebaro Klautau, Pedro Batista, Nuria González-Prelcic, Yuyang Wang, and Robert W Heath. 5g mimo data for machine learning: Application to beamselection using deep learning. In Proc. of ITA, pages 1–9. IEEE, 2018.
- [19] Manikanta Kotaru, Kiran Joshi, Dinesh Bharadia, and Sachin Katti. Spotfi: Decimeter level localization using WiFi. In Proc. of SIGCOMM, 2015.
- [20] Unwired Lab. Opencellid, 2020.
- [21] Yuanjie Li, Qianru Li, Zhehui Zhang, Ghufran Baig, Lili Qiu, and Songwu Lu. Beyond 5g: Reliable extreme mobility management. In Proc. of SIGCOMM, 2020.
- [22] Yuanjie Li, Chunyi Peng, Zengwen Yuan, Jiayao Li, Haotian Deng, and Tao Wang. Mobileinsight: Extracting and analyzing cellular network information on smartphones. In *Proc. of MobiCom*, pages 202–215, New York, NY, USA, 2016.
- [23] Run-Fa Liao, Hong Wen, Jinsong Wu, Huanhuan Song, Fei Pan, and Lian Dong. The rayleigh fading channel prediction via deep learning. Wireless Communications and Mobile Computing, 2018.
- [24] Lihong Liu, Hui Feng, Tao Yang, and Bo Hu. Mimo-ofdm wireless channel prediction by exploiting spatial-temporal correlation. *IEEE transactions on wireless* communications, 13(1):310–319, 2013.
- [25] Yunfei Ma, Nicholas Selby, and Fadel Adib. Minding the billions: Ultra-wideband localization for deployed rfid tags. In Proc. of ACM MobiCom, 2017.
- [26] James Munkres. Algorithms for the assignment and transportation problems. Journal of the society for industrial and applied mathematics, 5(1):32–38, 1957.
- [27] L Srikar Muppirisetty, Tommy Svensson, and Henk Wymeersch. Spatial wireless channel prediction under location uncertainty. IEEE Transactions on Wireless Communications, 15(2):1031–1044, 2015.
- [28] Rajalakshmi Nandakumar, Vikram Iyer, Desney Tan, and Shyamnath Gollakota. FingerIO: Using active sonar for fine-grained finger tracking. In Proc. of ACM CHI, pages 1515–1525, 2016.
- [29] Qifan Pu, Sidhant Gupta, Shyam Gollakota, and Shwetak Patel. Whole-home gesture recognition using wireless signals. In Proc. of ACM MobiCom, 2013.
- [30] Lenin S. Ravindranath, Calvin Newport, Hari Balakrishnan, and Samuel Madden. Improving Wireless Network Performance Using Sensor Hints. In Proc. of NSDI, Boston, MA, March 2011.
- [31] Patchava Raviteja, Khoa T. Phan, and Yi Hong. Embedded pilot-aided channel estimation for otfs in delay-doppler channels. IEEE Transactions on Vehicular Technology, 68:4906-4917, 2018.
- [32] D. Shutin and G. Kubin. Tracking and prediction of multipath components in wireless mimo channels. In Proc. of VTC, pages 329–333, 2007.
- [33] L. Sun, S. Sen, D. Koutsonikolas, and K. Kim. WiDraw: enabling hands-free drawing in the air on commodity WiFi devices. In Proc. of ACM MobiCom, 2015.
- [34] G. D. Surabhi, R. M. Augustine, and A. Chockalingam. On the diversity of uncoded offs modulation in doubly-dispersive channels. *IEEE Transactions on Wireless Communications*, 18(6):3049–3063, 2019.
- [35] Engineering Toolbox. Electrical conductivity of elements and other materials.
- [36] Engineering Toolbox. Relative permittivity dielectric constant.
- [37] International Telecommunication Union. Electrical characteristics of the surface of the earth. Recommendation ITU-R, P.527-3, 1992.
- [38] International Telecommunication Union. Effects of building materials and structures on radiowave propagation above about 100 mhz. Recommendation ITU-R, P.2040-1:22-23, 2015.
- [39] D. Vasisht, S. Kumar, H. Rahul, and D. Katabi. Eliminating channel feedback in next-generation cellular networks. In *Proc. of SIGCOMM*, 2016.
- [40] Jue Wang, Deepak Vasisht, and Dina Katabi. RF-IDraw: virtual touch screen in the air using RF signals. In Proc. of ACM SIGCOMM, 2014.
- [41] Song Wang, Jingqi Huang, and Xinyu Zhang. Demystifying Millimeter-Wave V2X: Towards Robust and Efficient Directional Connectivity Under High Mobility. In Proc. of ACM MobiCom, 2020.
- [42] Wei Wang, Alex X Liu, and Ke Sun. Device-free gesture tracking using acoustic signals. In Proc. of MobiCom, pages 82–94, 2016.
- [43] Teng Wei and Xinyu Zhang. mTrack: high precision passive tracking using millimeter wave radios. In Proc. of ACM MobiCom, 2015.
- [44] Ian C Wong and Brian L Evans. Spc03-4: Exploiting spatio-temporal correlations in mimo wireless channel prediction. In Proc. of IEEE Globecom, pages 1–5, 2006.
- [45] Yaxiong Xie, Jie Xiong, Mo Li, and Kyle Jamieson. Md-track: Leveraging multidimensionality for passive indoor wi-fi tracking. In Proc. of MobiCom, 2019.
- [46] Sangki Yun, Yi chao Chen, and Lili Qiu. Turning a mobile device into a mouse in the air. In Proc. of ACM MobiSys, May 2015.
- [47] Sangki Yun, Yi-Chao Chen, Huihuang Zheng, Lili Qiu, and Wenguang Mao. Strata: Fine-grained acoustic-based device-free tracking. In Proc. of MobiSys, 2017.
- [48] Yanzi Zhu, Yibo Zhu, Ben Y. Zhao, and Haitao Zheng. Reusing 60 GHz radios for mobile radar imaging. In Proc. of ACM MobiCom, 2015.